

Application of the complete multiple reciprocity method for 3D impedance extraction with multiple frequency points

Changhao Yan, Wenjian Yu*, Zeyi Wang

Department of Computer Science and Technology, Tsinghua University, Beijing 100084, China

Received 19 September 2005; accepted 10 March 2006

Available online 4 May 2006

Abstract

A complete multiple reciprocity method (CMRM), usually employed for the eigenvalue analysis of Helmholtz equation, is applied to impedance calculation of 3D electric structures for multiple frequency points. Based on a recently proposed boundary integral formulations for impedance calculation, the CMRM is used to separate the boundary integrals into the frequency-dependent and frequency-independent portions so as to accelerate the computation for multiple frequency points. A set of approaches is proposed to handle the severe numerical problems induced by the large varieties of distance r and frequency-dependent k , when applying the CMRM to impedance calculation. As a result, the near-field integrals are calculated with the inner product of a frequency-independent sequence and a frequency-dependent sequence, while the far-field integrals are calculated with an efficient approximate formula. Since the majority of the calculation for generating the overall linear equation system becomes reusable, the impedance extraction with multiple frequency points is greatly accelerated. Several typical structures of interconnects are calculated with the boundary element method combined with CMRM. Numerical results verify the accuracy and efficiency of the proposed methods.

© 2006 Elsevier Ltd. All rights reserved.

Keywords: Multiple reciprocity method; Boundary element method; Impedance extraction; Multiple frequency points; 3D VLSI interconnects

1. Introduction

The boundary element method (BEM) has been employed to solve various partial differential equations, including the Laplace equation, Poisson equation, and Helmholtz equation, in scientific and engineering applications. For the Helmholtz equation $\nabla^2 u + k^2 u = 0$ in a bounded domain, the conventional BEM formulation uses the complex-valued fundamental solution of the Helmholtz equation, which includes the wave number k [1]. This formulation is straightforward, but the k -dependent integral kernel leads to large computational time in applications where the boundary integrals need to be recomputed for different k values. The problem of eigenvalue analysis is such a case. And the similar situation is encountered in the impedance calculation (extraction) of

interconnect structures with multiple frequency points, which is the object of this paper.

The Helmholtz equation can also be transformed into several other kinds of BEM formulation, which do not employ the k -dependent complex-valued fundamental solution. The simplest one is to apply the real-valued fundamental solution of the Laplace equation, which only includes the distance r in the integral kernel. However, this formulation produces an additional domain integral due to the second term in the Helmholtz equation. Therefore, directly using it loses the spirit of BEM and is not efficient. A dual reciprocity method (DRM) was proposed to remedy this drawback, with the help of an additional application of Green's identity [2]. The DRM requires a special influence-type interpolation function to approximate the unknown function inside the domain and some internal points besides the boundary nodes [3,4]. The multiple reciprocity method (MRM), proposed by Nowak and Brebbia [5,6], employs a series of real-valued higher-order fundamental solutions of the Laplace equation instead of the Helmholtz fundamental solution. The main

*Corresponding author. Tel.: +86 10 62773440; fax: +86 10 62781489.

E-mail addresses: yanch02@mails.tsinghua.edu.cn (C. Yan),
yu-wj@tsinghua.edu.cn (W. Yu), wangzy@tsinghua.edu.cn (Z. Wang).

advantage of this method is that k can be left outside the boundary integral, which makes it convenient for recomputing the integrals for different k values.

However, directly using the MRM formulation may cause the spurious eigenvalue problem. Chen and Wong found out this phenomenon in one-dimensional (1D) and two-dimensional (2D) problems [7,8], and combined both singular and hypersingular equations for MRM to resolve it [7]. In Refs. [9,10], it was revealed that the kernels of the MRM are the real parts of the kernels in the complex-valued formulation of Helmholtz equation. Yeih et al. [11] then proved a clearer and more exact relationship between the MRM formulation and the complex-valued formulation, and proposed a complete MRM (CMRM), which is equivalent to the complex-valued formulation but holds the advantage of the original MRM. The CMRM solved the spurious eigenvalue problem perfectly, and was recently applied to 1D Helmholtz equation of semi-infinite domain [12].

Fast three-dimensional (3D) electro-magnetic simulation is increasingly important in the area of on-chip interconnect analysis, packaging, and microwave/RF engineering [13]. Fast and accurate computation of impedance (including inductance and resistance) of interconnect structures has become a research focus as the operating frequency of integrated circuits exceeds several giga-Hz (GHz, 10^9 Hz). To calculate the impedance, we need to know the current flowing through the conductor under a given bias voltage setting. A method introduced in [14], which discretizes the conductor volume, has gained the most popularity for the impedance extraction problem. However, the volume discretization method has to use very fine grids to handle problems with high frequency because some electro-magnetic effects induce a very irregular distribution of current in the conductor body. This makes the volume method very costly. Recently, a boundary integral equation (BIE) method was proposed for 3D impedance extraction [15,16], which overcomes the shortcomings of the volume-based method and is suitable for a wide-band simulation. Further numerical improvements were then proposed for this boundary integral formulation [17].

On the other hand, since the impedance is frequency-dependent, the values of impedance for multiple frequency points (within a frequency range) are usually needed, especially for the modeling of inductor components in RF circuits. The BEM for impedance extraction in [16], although with high efficiency for a single frequency, is still costly for the problem with multiple frequency points. It just converts the governing Helmholtz equations of the electro-magnetic field, into the conventional BEM formulation. Therefore, the k -dependent boundary integrals need to be recomputed for each different frequency; here k is a function of frequency f .

In this paper, the CMRM is applied to the area of impedance extraction of 3D structures, and combined with the BEM in [16] to accelerate the computation with

multiple frequency points. In theory, this is the application of CMRM to a boundary value problem (BVP) of the Helmholtz equation. While solving the vector Helmholtz equation of electric field \vec{E} in [16], the CMRM formulation is adopted to replace the conventional complex-valued formulation such that the computation of frequency-independent integrals can be reused. However, in the problems of impedance extraction, the distance r usually varies from several tens of nanometer (10^{-9} m) to several millimeters (10^{-3} m), and the frequency f varies for several magnitudes, up to 100 GHz. The large varieties of r and k , which were not encountered in existing literatures on MRM or CMRM, bring severe numerical difficulty to the CMRM formulation. To solve the problem induced by large variety of r , an average distance r_{avg} is introduced to make the CMRM formulation easily computed. Like the ill-conditioned series $\sum_{j=0}^N (-x)^j/j!$, handling the series of fundamental solutions in CMRM also suffers from the severe numerical cancelation. For this problem, a window technique is proposed to divide the CMRM integrals into near-field integrals and far-field integrals. The near-field integrals can be calculated as the partial summation of series in CMRM safely; the far-field integrals are calculated with a proposed efficient approximate formula, due to the equivalence of CMRM kernel to the complex-valued Helmholtz kernel. The criterion of the window is also proposed with physical meaning.

In numerical experiments, several interconnect structures are calculated with the BEM combined with the CMRM. Numerical results show that our method exhibits great speedup for 3D impedance extraction with many frequency points, while preserving high accuracy.

2. Review of the MRM and CMRM

In this section, we will briefly summarize the MRM and CMRM formulation of the 3D Helmholtz equation

$$\nabla^2 u + k^2 u = 0 \quad \text{in } \Omega, \quad (1)$$

where u is the field variable defined in a 3D closed domain Ω surrounded by the boundary Γ , and k is the wave number. If employing the complex-valued fundamental solution of the Helmholtz equation, Eq. (1) can be transformed into the following BIE with respect to a source point s on Γ [1]:

$$c_s u_s + \int_{\Gamma} (u q_H^* - q u_H^*) d\Gamma = 0, \quad (2)$$

where u_s denotes the value of field variable on source point s , c_s is a constant depending on the geometry of boundary at s . $q = \partial u / \partial n$ is the normal derivative of u on the boundary; here n denotes the outward normal direction of the boundary. The complex fundamental solution of the Helmholtz equation u_H^* is $e^{-ikr}/4\pi r$, where r is the distance between a field point and source point s . q_H^* is defined as $\partial u_H^* / \partial n$.

Instead, if only applying the fundamental solution of the Laplace equation $u_0^* = 1/4\pi r$ and $q_0^* = \partial u_0^*/\partial n$, one can obtain the integral equation as follows:

$$c_s u_s + \int_{\Gamma} (u q_0^* - q u_0^*) d\Gamma = k^2 \int_{\Omega} u u_0^* d\Omega. \quad (3)$$

The MRM formulation further adopts the higher-order fundamental solutions of the Laplace equation:

$$\nabla^2 u_{j+1}^* = u_j^* = \frac{1}{4\pi r} \frac{r^{2j}}{(2j)!}, \quad q_j^* = \frac{\partial u_j^*}{\partial n}, \quad j = 0, 1, 2, \dots, \quad (4)$$

to transform the right side domain integral in Eq. (3). Substituting Eq. (4) with $j = 0$ into the right-hand side of Eq. (3), using the Green's identity, one obtains

$$\int_{\Omega} u u_0^* d\Omega = \int_{\Gamma} (u q_1^* - q u_1^*) d\Gamma - k^2 \int_{\Omega} u u_1^* d\Omega. \quad (5)$$

Therefore, Eq. (3) can be rewritten as

$$\begin{aligned} c_s u_s + \int_{\Gamma} (u q_0^* - q u_0^*) d\Gamma - k^2 \int_{\Gamma} (u q_1^* - q u_1^*) d\Gamma \\ = k^2 (-k^2) \int_{\Omega} u u_1^* d\Omega. \end{aligned} \quad (6)$$

Then, N similar transformations lead to

$$\begin{aligned} c_s u_s + \sum_{j=0}^N (-k^2)^j \left[\int_{\Gamma} (u q_j^* - q u_j^*) d\Gamma \right] \\ = (-1)^N (k^2)^{N+1} \int_{\Omega} u u_N^* d\Omega \approx 0. \end{aligned} \quad (7)$$

If r and k are bounded, for sufficiently large N , the domain integral in Eq. (7) becomes negligible and can be dropped [5,6,18]. This is the basic formulation of the MRM.

The MRM, in which both u_j^* and q_j^* are real-valued, may encounter the spurious eigenvalue problem [7,8]. Besides, it cannot be used to solve the Helmholtz equation with an infinite domain directly. To solve these problems, an appropriate complex constant is introduced into the zeroth-order fundamental solution in Eq. (4). The derived formulation is called CMRM. The j th-order fundamental solution in the CMRM is [11]¹:

$$\bar{u}_j^* = \frac{1}{4\pi} \left[\frac{1}{r} \frac{r^{2j}}{(2j)!} - ik \frac{r^{2j}}{(2j+1)!} \right], \quad j = 0, 1, 2, \dots \quad (8)$$

With the similar derivation to that for MRM, the integral equation of CMRM is obtained:

$$c_s u_s + \int_{\Gamma} (u \bar{q}^* - q \bar{u}^*) d\Gamma = 0, \quad (9)$$

where

$$\bar{u}^* = \sum_{j=0}^N (-k^2)^j \bar{u}_j^*, \quad \bar{q}^* = \sum_{j=0}^N (-k^2)^j \bar{q}_j^*, \quad (10)$$

and $\bar{q}_j^* = \partial \bar{u}_j^*/\partial n$. The series in Eq. (10) simply converges to the corresponding kernel in the complex-valued formulation of Helmholtz equation [11].

3. BEM for 3D impedance extraction

Fig. 1 shows a 3D structure including M interconnect conductors. The impedance of this system of conductors is defined as a Z matrix, which fulfills $ZI = V$. Here, I and V are the vectors of current through the conductor and voltage between two ends (contacts) of conductor, respectively. To calculate the frequency-dependent impedance matrix, a set of sinusoidal voltages V at frequency f is imposed on the conductors, with one of them being complex $1V$ and the others 0. Then, the problem of impedance extraction becomes to compute the current in each conductor by solving the electro-magnetic equations. Once the currents are obtained, we denote them as a column vector, say I_1 . Then, changing the conductor voltage setting and computing corresponding currents of conductors repeatedly, one can obtain the current vectors I_2, \dots, I_M . Finally, with the obtained current matrix $I = [I_1, I_2, \dots, I_M]$, we have $ZI = \mathbf{1}$, where $\mathbf{1}$ is the identity matrix. So, the impedance matrix becomes [14–16]:

$$Z = I^{-1} \quad \text{and} \quad R = \text{real}(Z), \quad L = \text{imag}(Z)/i\omega.$$

R and L are the resistance and inductance matrix, respectively. And ω is the angular frequency, $\omega = 2\pi f$. Now, the key problem of impedance extraction is how to compute the currents in conductors for a given voltage set.

Ref. [16] proposed a set of surface integral formulae for 3D impedance extraction under magneto-quasistatic (MQS), electro-magneto-quasistatic (EMQS) assumption and even full-wave analysis. For simplicity, we only discuss the MQS simulation in this paper and list the differential equations and corresponding BIEs in Table 1. In this table, \vec{E} is electric field vector, φ is electric potential, \vec{E}_t denotes tangential component of \vec{E} . \vec{J} is current density vector, and \vec{A} is magnetic vector potential. The vector Helmholtz equation in Table 1:

$$\nabla^2 \vec{E} - i\omega\mu\sigma \vec{E} = 0 \quad (11)$$

is the most important, which can be decomposed into three scalar Helmholtz equations under the Cartesian coordinate system. In the Helmholtz equations, μ and σ are the

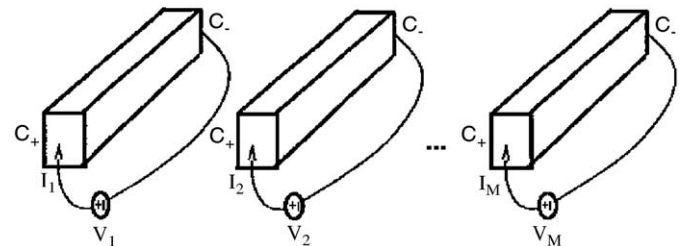


Fig. 1. Multi-conductor structure for impedance extraction [16].

¹There is a typo in Ref. [11], which loses a k in the imaginary term.

Table 1
Differential and boundary integral formulations for 3D impedance extraction under MQS assumption [16]

	Governing differential equations	Boundary integral equations
For domain in each conductor	$\nabla^2 \vec{E} - i\omega\mu\sigma \vec{E} = 0$	$\rightarrow \int G_1(\mathbf{x}, \mathbf{y}) \frac{\partial \vec{E}(\mathbf{y})}{\partial n_y} d\mathbf{y} - \int \frac{\partial G_1(\mathbf{x}, \mathbf{y})}{\partial n_y} \vec{E}(\mathbf{y}) d\mathbf{y} = \frac{1}{2} \vec{E}(\mathbf{x})$
	$\nabla \cdot \vec{E} = 0$	$\rightarrow \int_c E_t(\mathbf{x}) \cdot (\vec{n}(\mathbf{x}) \times \vec{l}(\mathbf{x})) d\mathbf{x} - \int_a \frac{\partial E_n(\mathbf{y})}{\partial n_y} d\mathbf{y} = 0$
For medium domain	$\nabla^2 \vec{E} = i\omega\mu \vec{J}$	$\rightarrow \int_s G_0(\mathbf{x}, \mathbf{y}) \frac{\partial \vec{E}(\mathbf{y})}{\partial n_y} d\mathbf{y} - \int_s \frac{\partial G_0(\mathbf{x}, \mathbf{y})}{\partial n_y} \vec{E}(\mathbf{y}) d\mathbf{y} + \nabla\phi(\mathbf{x}) = 0$
	$-\nabla\phi = \vec{E} + i\omega \vec{A}$	
	$\vec{A} = \int \mu G_0(\mathbf{x}, \mathbf{y}) \vec{J}(\mathbf{y}) d\mathbf{y}$	
On noncontact surface		$E_n = 0$
On contact surface		$\begin{cases} \phi(\mathbf{x}) = \text{constant} \\ \frac{\partial E_n(\mathbf{x})}{\partial n_x} = 0 \end{cases}$

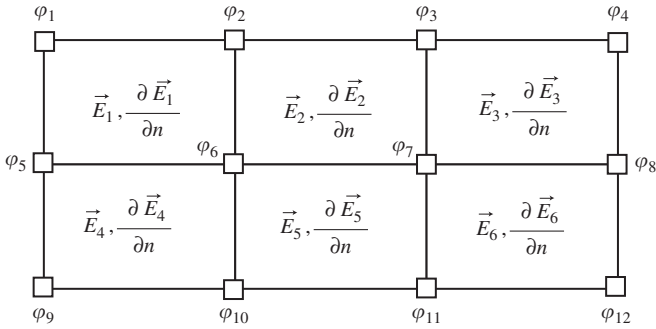


Fig. 2. The discretization of conductor surface.

permeability and conductivity of material, respectively, and both are constant. The complex-valued fundamental solution of Helmholtz equation was adopted to transform the Helmholtz equation into the BIE, in [16]. This fundamental solution is denoted by $G_1(\mathbf{x}, \mathbf{y})$ in Table 1, where \mathbf{x} is source point, and \mathbf{y} is field point for integration. $G_0(\mathbf{x}, \mathbf{y})$ is the Laplace fundamental solution.

To solve the equations in Table 1, the conductor surfaces are discretized into panels with constant interpolation function. Then, evaluating the discretized BIE at every collocation point, one for an panel, one can get the corresponding linear equations. With other discretizing techniques, the whole equations in Table 1 are considered and coupled with each other to form an overall linear equation system $Ax = b$. In this linear equation system, the \vec{E} and $\partial \vec{E} / \partial n$ on panel, and ϕ on vertex are the unknowns to be solved. Fig. 2 shows a surface discretization with six panels, and the discretized unknowns are labeled in it.

To set up the matrix A , the major work is computing the coefficients in the discretized BIE transformed from Eq. (11):

$$\begin{cases} P_1(a, b) = \int_{panel_b} \frac{e^{-ikr(\mathbf{x}_a, \mathbf{y})}}{4\pi r(\mathbf{x}_a, \mathbf{y})} d\mathbf{y}, \\ D_1(a, b) = \int_{panel_b} \frac{\partial}{\partial n_y} \left[\frac{e^{-ikr(\mathbf{x}_a, \mathbf{y})}}{4\pi r(\mathbf{x}_a, \mathbf{y})} \right] d\mathbf{y}, \end{cases} \quad (12)$$

where a, b are the global indexes of the panels, $panel_b$ is the b th panel, and $k = \sqrt{-i2\pi f\mu\sigma}$. \mathbf{x}_a stands for the collocation point in the a th panel, and the operator $r(\cdot)$ calculates the distance between two points.

Since this formulation includes the frequency-dependent integral kernel, it becomes inefficient for impedance extraction with multiple frequency points. Both MRM and CMRM seems applicable for this BVP of Helmholtz equation with finite domain, to make the f outside the integral so as to accelerate the computation with multiple frequencies. However, it is found out that only CMRM is practical for the application in this paper, which will be explained in Section 4.4.

When applying the CMRM, we can replace the P_1 and D_1 in (12) with P^* and D^* , respectively:

$$P^*(a, b) = \int_{panel_b} \bar{u}^* d\mathbf{y}, \quad D^*(a, b) = \int_{panel_b} \bar{q}^* d\mathbf{y}, \quad (13)$$

where \bar{u}^* and \bar{q}^* are defined in Eq. (10). Therefore, with removing the frequency f from the integral and choosing an appropriate truncation number N , the boundary integrals become frequency-independent and can be reused for different frequency values.

4. Applying the CMRM to 3D impedance extraction

When applying CMRM to the impedance extraction of 3D interconnects within a frequency range, the wide varieties of frequency f and distance r bring difficulties to the computation of the integrals of CMRM series. Below, we will discuss the difficulties in detail and propose a set of approaches to resolve them with reasonable efficiency.

4.1. Introducing an average distance to the formula

When calculating the coefficients $P^*(a, b)$ and $D^*(a, b)$ in (13) with the CMRM formulation of (8) and (10), severe numerical difficulties will occur. Below, we consider the first part of \bar{u}_j^* in (8) as an example, without loss of generality. When it is substituted into Eqs. (10) and (13),

we get the following integral for computation:

$$\begin{aligned} P_1^*(a, b) &= \int_{\text{panel}_b} \sum_{j=0}^N (-k^2)^j \left[\frac{1}{4\pi r(\mathbf{x}_a, \mathbf{y})} \cdot \frac{r(\mathbf{x}_a, \mathbf{y})^{2j}}{(2j)!} \right] d\mathbf{y} \\ &= \sum_{j=0}^N (-k^2)^j \int_{\text{panel}_b} \left[\frac{1}{4\pi r(\mathbf{x}_a, \mathbf{y})} \cdot \frac{r(\mathbf{x}_a, \mathbf{y})^{2j}}{(2j)!} \right] d\mathbf{y}. \end{aligned} \quad (14)$$

To separate the frequency-dependent and frequency-independent portions, $P_1^*(a, b)$ is not directly calculated by (14). In fact, it is divided into two sequences as follows:

$$P_{1k,j}^* = (-k^2)^j, \quad (15)$$

$$P_{1r,j}^* = \int_{\text{panel}_b} \frac{1}{4\pi r(\mathbf{x}_a, \mathbf{y})} \cdot \frac{r(\mathbf{x}_a, \mathbf{y})^{2j}}{(2j)!} d\mathbf{y}. \quad (16)$$

The frequency-independent sequence (16) including the arduous integral operator can be computed and saved in advance. Then, one obtains $P_1^*(a, b)$ by the following inner product:

$$P_1^*(a, b) = \sum_{j=0}^N P_{1k,j}^* \cdot P_{1r,j}^*(a, b). \quad (17)$$

In sequence $P_{1r,j}^*$, the power term r^{2j} will cause a numerical problem. For example, for the interconnect structures in integrated circuits, the value of r is not only very small but with a large variety. In the unit of meter, the value of r may vary from about 10^{-7} to 10^{-4} . Directly computing the term $r(\mathbf{x}_a, \mathbf{y})^{2j}$ in $P_{1r,j}^*(a, b)$ will cause the underflow problem even while j is not very large. This is greatly different from the applications of MRM or CMRM in existing literatures, where r was about 1.0.

To solve the problem induced by the value of r only, we introduce an *average* distance r_{avg} to modify the CMRM formulation. Therefore, the formula (14) will be transformed into

$$\begin{aligned} P_1^*(a, b) &= \sum_{j=0}^N (-1)^j (kr_{avg})^{2j} \int_{\text{panel}_b} \frac{1}{4\pi r(\mathbf{x}_a, \mathbf{y})} \cdot \frac{r_{rel}(\mathbf{x}_a, \mathbf{y})^{2j}}{(2j)!} d\mathbf{y}, \end{aligned} \quad (18)$$

where $r_{rel}(\mathbf{x}_a, \mathbf{y}) = r(\mathbf{x}_a, \mathbf{y})/r_{avg}$. This r_{avg} is chosen to be the average of the distances between all vertexes of the integral panel and the collocation point:

$$r_{avg}(a, b) = \frac{1}{N_b} \sum_{t=1}^{N_b} r(\mathbf{x}_a, \mathbf{y}_{b,t}), \quad (19)$$

where \mathbf{x}_a is the collocation point on panel a , $\mathbf{y}_{b,t}$ is the t th vertex of panel b , N_b is the number of vertices on the panel b . Therefore, the $r_{rel}(\mathbf{x}_a, \mathbf{y})$ becomes near to 1, and thus

$$P_{1r,j}^*(a, b) = \int_{\text{panel}_b} \frac{1}{4\pi r(\mathbf{x}_a, \mathbf{y})} \cdot \frac{r_{rel}(\mathbf{x}_a, \mathbf{y})^{2j}}{(2j)!} d\mathbf{y} \quad (20)$$

can be calculated with much less difficulty within a small truncation number N of series. Note that $r_{avg}(a, b)$ is a

matrix indeed in our program implementation. We compute these *average* distances among any two panels, and then store them in a matrix.

4.2. A window technique to separate the near-field integral and far-field integral

With the introduction of r_{avg} , the formula we use to compute $P_1^*(a, b)$ becomes

$$P_1^*(a, b) = \sum_{j=0}^N P_{1k,j}^* \cdot P_{1r,j}^*(a, b), \quad (21)$$

where

$$P_{1k,j}^*(a, b) = (-1)^j [kr_{avg}(a, b)]^{2j} \quad (22)$$

and the definition of $P_{1r,j}^*(a, b)$ is given as Eq. (20). Now, $P_{1r,j}^*(a, b)$ can be calculated accurately. But the numerical difficulty still exist because of the large variety of $P_{1k,j}^*(a, b)$. For on-chip structures, usually copper is used as interconnect wire with conductivity $\sigma = 5.8 \times 10^7$ S/m. And the magnetic permeability in Eq. (11) has the value $\mu = 12.57 \times 10^{-7}$ H/m. For a wide-band simulation, the frequency f usually varies for several magnitudes, say, from 10^4 to 10^{11} Hz (100 GHz). Therefore, the norm of k ($= \sqrt{-i2\pi f \mu \sigma}$) in our consideration varies from about 10^3 to 10^6 . The norm of kr_{avg} still varies from about 10^{-3} to 10^2 . If the norm of kr_{avg} is large enough, say larger than 10, directly computing $P_1^*(a, b)$ with (21) will suffer from the numerical cancelation and cannot produce an accurate result. This is similar to the famous numerical problem of calculating e^{-x} with

$$e^{-x} = \lim_{N \rightarrow +\infty} \sum_{j=0}^N \frac{(-x)^j}{j!},$$

when x is a large positive number [19,20]. In other words, the summation of $N+1$ terms in (21) would not be computed with sufficient accuracy, unless the norm of kr_{avg} is small.

Our solution for this problem is a window technique to divide the integrals in (13) into near-field integrals and far-field integrals, and compute them with different methods, respectively. For a specified k , the near-field integral denotes the integrals in (13) with appropriate panel position such that $\|kr_{avg}(a, b)\| < W$ holds. The left integrals on other panels are called the far-field integral. Here W is a threshold value, with the meaning of window size. Because the restriction of kr_{avg} 's value can effectively reduce the numerical problem induced mainly by $P_{1k,j}^*$, the near-field integrals can then be computed accurately with the CMRM formulation. While for the far-field integrals, the CMRM formulation cannot be applied in practice, we propose another efficient approach and discuss it in Section 4.4.

Below, we will reveal some physical meaning of $kr_{avg}(a, b)$. For the impedance extraction under MQS

assumption, $k = (1 - i)k_{real}$ and

$$k_{real} = \sqrt{\frac{\omega\mu\sigma}{2}} = \frac{1}{\delta},$$

where δ is the skin depth characterizing the high-frequency effect, therefore,

$$kr_{avg} = \sqrt{2} \frac{r_{avg}}{\delta}. \tag{23}$$

It is related with the ratio of the average distance between the integral panel and the source point to the skin depth, which is a nondimensional quantity.

In practice, if we let $W = 2\pi$, the cancelation problem in computing (21) will be negligible and an accurate result can be obtained with $N = 11$. The electro-magnetic wave theory shows that the amplitude attenuation becomes less than 1% where the field point is five times skin depth away from the source [21]. Therefore, with $W = 2\pi$, the far-field integral could be computed in a coarse way since the electro-magnetic field there, due to the source, becomes very weak.

4.3. Computing the near-field integral

To calculate the integral of (13) accurately, a 2D Gauss–Legendre integration scheme is employed, which converts the problem to evaluating the integral kernel at some Gauss points. For the near-field integral, we use a recursive formula of the CMRM series instead of computing it directly. Taking the integrand of (20) as an example, the recursive formulation is

$$F_{1rj} = \frac{1}{4\pi r} \cdot \frac{r_{rel}^{2j}}{(2j)!} = \frac{r_{rel}^2}{(2j)(2j-1)} \cdot F_{1rj-1}$$

and $F_{1r,0} = 1/4\pi r$.

Moreover, in order to accelerate the computation, the coefficient $1/(2j)(2j-1)$ can be computed and saved in a table. Finally, when computing on a Gauss point, only two additional multiplication operations are needed for each term of the series. This technique greatly reduces the computational time for calculating the near field integrals of the CMRM series.

Besides, when the source point lies in the integrated panel, both $\int_{panel_b} \bar{u}_1^* dy$ and $\int_{panel_b} \bar{q}_1^* dy$ for computing $P^*(a, b)$ and $D^*(a, b)$ in (13) involve singular integrals. Special treatments for singular integrals are adopted to guarantee accuracy [22].

In above discussions, only the first part of CMRM formula (8) is considered as an example. While considering the second part of (8) together, the problems encountered are almost the same and this technique is still valid.

4.4. Computing the far-field integral

As mentioned in Section 4.2, the far-field integral could be computed in a coarse way. This is accomplished by the following direct approximation to the integral of complex-

valued Helmholtz kernel:

$$\begin{aligned} P^*(a, b) &= \frac{1}{4\pi} \int_{panel_b} \frac{e^{-ikr(x_a, y)}}{r(x_a, y)} dy \\ &\approx e^{-ikr_{avg}(a, b)} \int_{panel_b} \frac{1}{4\pi r(x_a, y)} dy \\ &= e^{-ikr_{avg}(a, b)} P_{1r,0}^*(a, b). \end{aligned} \tag{24}$$

Notice that this approximate formulation includes the arduous $e^{-ikr_{avg}(a, b)}$, but it is computed once for distance $r_{avg}(a, b)$, not for all Gauss points as needed in computing $P^*(a, b)$ accurately with the direct method. Moreover, the $P_{1r,0}^*(a, b)$ is right the first term of the series $P_{1r,j}^*(a, b)$, therefore no additional integral computation is needed. So, this approximating formula has very high computational efficiency.

In the same manner, we obtain the approximation to $D^*(a, b)$:

$$\begin{aligned} D^*(a, b) &= \frac{\partial P^*(a, b)}{\partial n} \\ &\approx e^{-ikr_{avg}(a, b)} \cdot \frac{\partial P_{1r,0}^*(a, b)}{\partial n} \\ &= e^{-ikr_{avg}(a, b)} \cdot D_{1r,0}^*(a, b), \end{aligned} \tag{25}$$

where $D_{1r,0}^*(a, b) = (\partial/\partial n) \int_{panel_b} 1/4\pi r(x_a, y) dy$.

To reveal the rationality of above approximate formulae for far-field integral, let us consider the integrand in $P^*(a, b)$:

$$\begin{aligned} \frac{1}{4\pi} \cdot \frac{e^{-ikr(x_a, y)}}{r(x_a, y)} &= \frac{e^{-(1+i)k_{real}r(x_a, y)}}{4\pi r(x_a, y)} \\ &= \frac{e^{-k_{real}r(x_a, y)} e^{-ik_{real}r(x_a, y)}}{4\pi r(x_a, y)}, \end{aligned} \tag{26}$$

where k_{real} is a positive number. If two panels a, b satisfy $\|kr_{avg}(a, b)\| > W$, then $k_{real}r(x_a, y) > W'$ and W' is a positive number near $W/\sqrt{2}$, for most Gauss points y . The attenuation term $e^{-k_{real}r(x_a, y)}$ in (26) makes the $P^*(a, b)$ of far-field integral much smaller than the near-field integral. Therefore, this approximate formulas (24) and (25) are reasonable, especially for a suitable value of W .

On the other hand, the MRM formulation does not hold the above feature. For example, the corresponding $P^*(a, b)$, with MRM formulation of (4), will become [10]:

$$u^* = \sum_{j=0}^N (-k^2)^j u_j^* \rightarrow \frac{1}{4\pi} \frac{\cos(kr(x_a, y))}{r(x_a, y)}.$$

With the increase of r , $\cos(kr(x_a, y))/r(x_a, y)$ dose not approach to zero because the k here used is a complex number. Numerical experiments also show that the $P^*(a, b)$ of far field is even larger than the one of near field, if using the MRM formulation.

The conventional MRM is not suitable for 3D impedance extraction of VLSI interconnects, because it still holds the same numerical difficulties of CMRM discussed in Sections 4.1 and 4.2, and there is no efficient approach

for far-field integrals of MRM by now. This answers the question why we choose the CMRM in this paper.

5. Numerical results

The proposed method based on the CMRM and the original direct BEM [16] for impedance extraction are both implemented in C++ language. In our experiments, the former is denoted by the CMRM and the latter by the ODBEM. For the ODBEM and CMRM, the generated linear systems are both solved with the Matlab backslash operator. In the experiments, two interconnect structures are extracted for the frequency-dependent impedances. The conductor surfaces are discretized into constant rectangular panels, with collocation point located in the center of each panel. To guarantee the accuracy of near singular integrals, a 2D Gauss–Legendre integral scheme with 20 × 20 Gauss points is used.

In the CMRM, we set $W = 2\pi$ and the series length $N = 12$. All programs are run on a PC with a Intel Pentium IV 1.8 GHz CPU.

5.1. A single wire

The dimensions of the first example are $1\ \mu\text{m} \times 1\ \mu\text{m} \times 8\ \mu\text{m}$ ($\mu\text{m} = 10^{-6}\ \text{m}$), and the surface of this conductor is discretized into 160 panels as shown in Fig. 3, where the red panels surrounding the two ends are for summing up the conductor current with the approach for high frequency [16]. The impedance of the wire is calculated with the ODBEM, CMRM, and FastHenry [23], a famous prototype of MIT using the volume discretization method, for the frequency range from 10^4 to 10^{11} Hz. The computa-

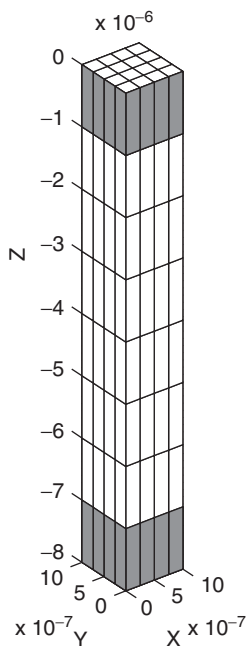


Fig. 3. A single rectangle wire.

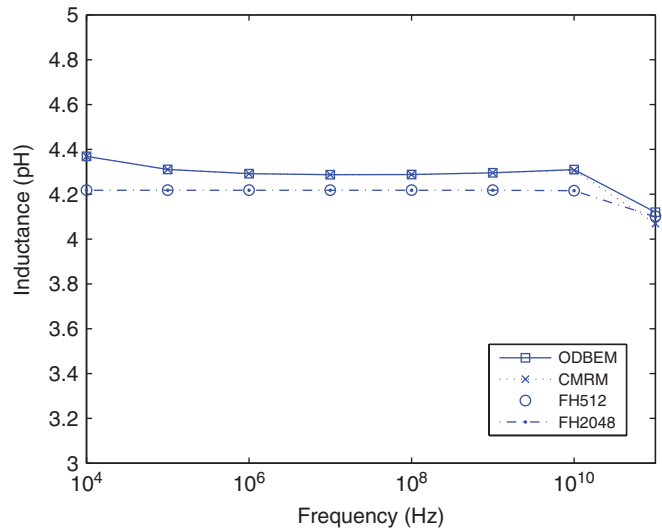


Fig. 4. Inductance.

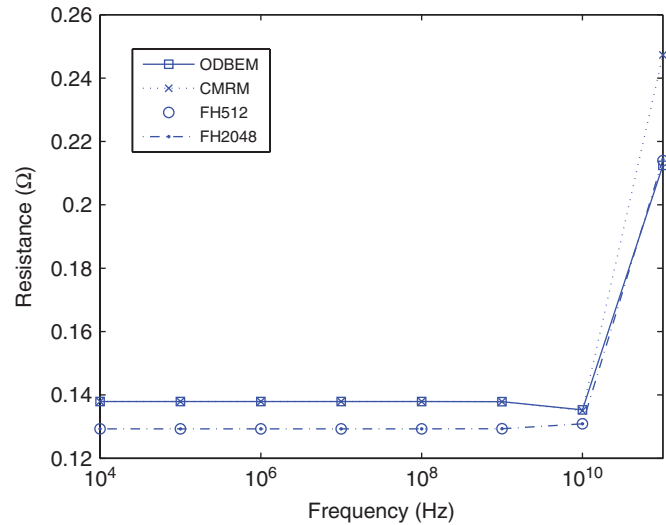


Fig. 5. Resistance.

tional results are shown in Figs. 4 and 5. The results of FastHenry with two different discretization are shown. For example, we use “FH512” to denote the FastHenry’s result with the discretization of 512 filaments.

From Fig. 4, we can see that the inductances obtained by the CMRM and ODBEM coincide with each other very well on the whole frequency range, and the difference of results from CMRM and FastHenry is less than 3.6%. While for the resistance, the results of CMRM are also close with those from other methods except the maximum relative discrepancy is about 15%, which occurs at the highest frequency $f = 100\ \text{GHz}$ (see Fig. 5). If frequency is 100 GHz, the threshold distance distinguishing the near-field and far-field integrals becomes $r_w = 0.93\ \mu\text{m}$. This distance is not sufficient to guarantee the accuracy of far-field integrals, and causes the large error in computing the resistance. However, the operating frequency of the VLSI circuit seems impossible to rise to 100 GHz in the near future. Besides, we have simulated the structure with

$f = 15$ GHz, the results match with other methods very well. Therefore, the CMRM is reliable and fulfills the requirements in current VLSI designs.

For speed comparison, the total CPU times of the CMRM and ODBEM are plotted in Fig. 6, versus the number of sampling frequency points. As shown in Fig. 6, the CMRM shows a very gentle increase in computing time compared with the ODBEM, as the number of frequency points increases. Besides, even for the first frequency point, the CMRM is a little faster than ODBEM, because of the efficient far-field integral formulation and computation of the CMRM series with the recursive formula. In this example, the frequency extends from 10^4 to 10^{11} Hz, including eight sample points, and the CMRM finally exhibits about three times speedup to the ODBEM.

In order to compare the speed of the ODBEM and CMRM in detail, we firstly list the main steps of both methods as follows:

- (i) Calculate the integrals related with the Laplace fundamental solution, i.e. the $G_0(\mathbf{x}, \mathbf{y})$ in Table 1.
- (ii) Calculate the integrals related with the Helmholtz fundamental solution, i.e. the $G_1(\mathbf{x}, \mathbf{y})$ in Table 1.
- (iii) Generate an overall linear equation system.
- (iv) Solve the linear equation system, and calculate the impedance.

The difference between the ODBEM and CMRM only lies in step (ii). The ODBEM directly computes the numerical integrals of complex-valued fundamental solutions. In contrast, the CMRM calculates the far-field integrals with approximate formulae (24) and (25), while dividing the near-field integrals into the following three steps:

- (i) Compute the r_{avg} matrix.
- (ii) Calculate and save the frequency-independent series, such as the $P_{1r,j}^*(a, b)$ in (20).

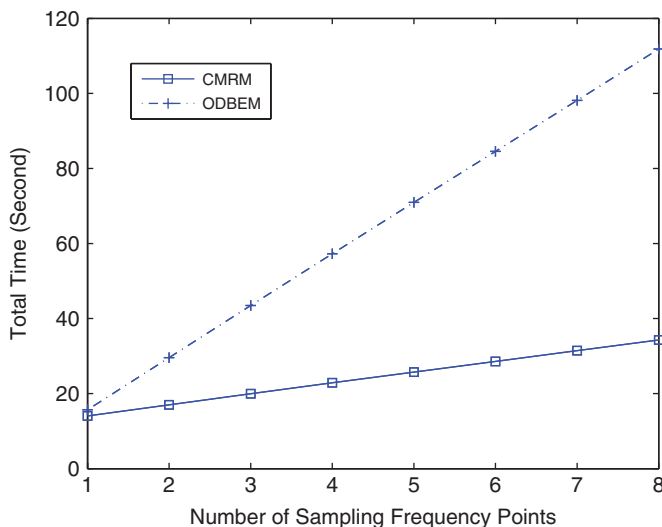


Fig. 6. CPU time comparison.

- (iii) Sum up the frequency-independent series with the frequency-dependent coefficients, as (21).

In the CMRM, only the third step above is needed to repeat for different frequencies, besides the far-field integrals. While with the ODBEM, the whole step (ii) needs to run repeatedly for different frequency.

To illustrate this point more clearly, the CPU time of each step for calculating impedance for a single frequency point is listed in Table 2, where the symbol asterisk indicates the step that should be recomputed for every different frequency point. From Table 2, we can see that the time of calculating the Helmholtz integrals is about seven times (11.141 s/1.766 s) of that for the Laplace integrals. This is due to the more complexity of the kernel e^{-ikr}/r than $1/r$. Specially, from the second frequency point, the CPU time of the Helmholtz integrals in CMRM is only 0.156 s for reusing the integrals among different frequencies, while the ODBEM still needs 11.141 s. This shows the reason why the CMRM is faster than the ODBEM on the extraction of multiple frequency points.

5.2. A 1 × 1 crossover

The second example is a 1 × 1 crossover structure shown in Fig. 7. The numbers of panels and unknowns involved are 320 and 2244, respectively. We set frequency $f = 15$ GHz, and run CMRM with different values of W and N to investigate the relationship between the computational accuracy and the two parameters. The self-inductances and resistances of a conductor are listed in Table 3. Taking the ODBEMs result as the standard, the relative errors of R and L are also listed for different settings of W and N .

From Table 3, we can see that at this high frequency of 15 GHz, even if $N = 5$, the inductance computed by CMRM can hold the relative error less than 3%. With this small value of N , the CMRM spends much less memory than the situation in Section 5.1. On the other hand, the resistance is more sensitive to the value of W than inductance. Anyway, with $W = 2\pi$ and $N = 9$, both R and L have relative errors less than 3%, which are sufficient for the VLSI simulation.

For the calculation of this structure at many frequency points, a large speedup ratio of CMRM to ODBEM is also revealed, just like that for the first example.

Table 2
CPU time of the single wire example (s)

	Laplace integral	Helmholtz integral	Generate $Ax = b$	Solve $Ax = b$
ODBEM		11.141*		
	1.766	r_{avg}	Series	Sum up
CMRM		0.000	9.234	0.156*

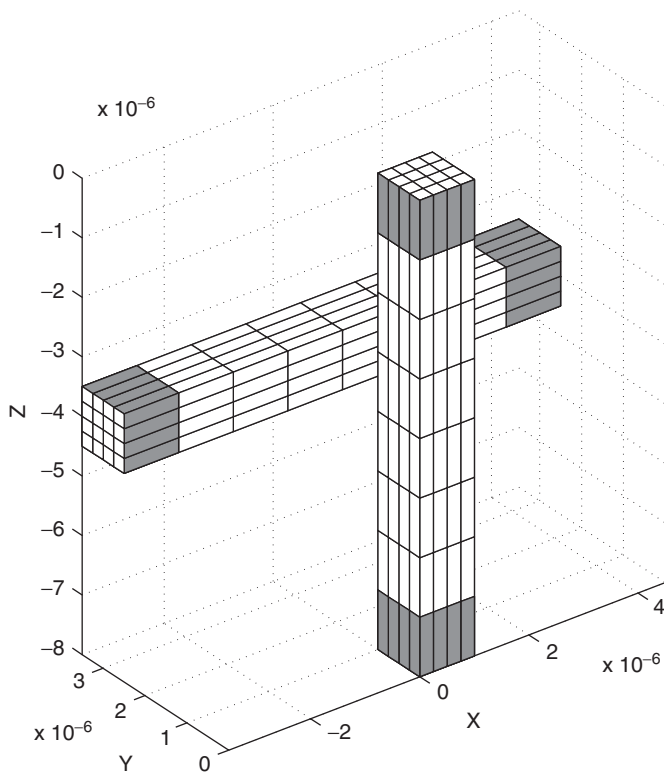


Fig. 7. A 1×1 crossover structure.

Table 3

The computational results of self-inductance and resistance for the 1×1 crossover with different values of (N, W)

(N, W)	$R (\Omega)$	Error (%)	$L (10^{-12} \text{ H})$	Error (%)
$(12, 2\pi)$	0.143694	-0.0	4.21306	-0.0
$(9, 2\pi)$	0.147152	2.4	4.18193	-0.8
$(7, \pi)$	0.157814	9.8	4.31280	2.3
$(6, \pi)$	0.157947	9.9	4.31319	2.4
$(5, \pi)$	0.158561	10.3	4.30941	2.3
ODBEM	0.143738	-	4.21392	-

6. Conclusions

The 3D impedance extraction with multiple frequency points has become an important issue for the VLSI or microwave/RF engineering. Based on a recently proposed boundary integral formulation for wide-band impedance extraction, the CMRM is applied to greatly reduce the computational expense in generating the overall linear systems for multiple frequency points. To solve the severe numerical problems induced by the large varieties of r and k , which are not mentioned in existing literatures of the MRM or CMRM, a set of approaches is proposed. The boundary integrals are divided into the near-field integrals and far-field integrals. The near-field integrals are calculated with the CMRM formulae in the power series form

safely, while the far-field integrals are calculated with an efficient approximate formula. In numerical experiments, the efficiency of proposed approaches is verified. Compared with the original BEM, which simply repeats the computation for different frequency points, the proposed CMRM has gained a large speedup while preserving desirable accuracy.

Acknowledgments

The authors would like to thank Prof. J.T. Chen, Dr. W. Yeih of Taiwan Ocean University for helpful discussion. The authors also wish to express their thanks for financial support from the National Science Foundation of China under Contract no. 90407004.

References

- [1] Kleinman RE, Roach GF. Boundary integral equations for the three-dimensional Helmholtz equation. *SIAM Rev* 1974;16:214–36.
- [2] Nardini D, Brebbia CA. A new approach to free vibration analysis using boundary element method. Proceedings of the fourth international conference bound elements, 1982. p. 313–26.
- [3] Partridge PW, Brebbia CA. The dual reciprocity boundary element method for the Helmholtz equation. Proceedings of the international bound elements symposium, 1990. p. 543–55.
- [4] Ali A, Rajakumar C, Yunus SM. On the formulation of the acoustic boundary element eigenvalue problems. *Int J Numer Meth Eng* 1992;31:1271–82.
- [5] Nowak AJ, Brebbia CA. Solving Helmholtz equation by boundary elements using the multiple reciprocity method. *Comput Exp Fluid Flow* 1989;265–70.
- [6] Nowak AJ, Brebbia CA. The multiple reciprocity method—a new approach for transforming BEM domain integrals to the boundary. *Eng Anal Bound Elem* 1989;6:164–7.
- [7] Chen JT, Wong FC. Analytical derivations for one-dimensional eigenproblems using dual boundary element method and multiple reciprocity method. *Eng Anal Bound Elem* 1997;20:25–33.
- [8] Wong FC. Analysis and experiment for acoustic modes of a cavity containing an incomplete partition. Master thesis, National Taiwan Ocean University, Taiwan; 1997.
- [9] Kamiya N, Andoh E, Nogae K. A new complex-valued formulation and eigenvalue analysis of the Helmholtz equation by boundary element method. *Adv Eng Software* 1996;26:219–27.
- [10] Kamiya N, Andoh E, Nogae K. Three-dimensional eigenvalue analysis of the Helmholtz equation by multiple reciprocity boundary element method. *Adv Eng Software* 1993;16:203–7.
- [11] Yeih W, Chen JT, Chen KH, Wong FC. A study on the multiple reciprocity method and complex-valued formulation for the Helmholtz equation. *Adv Eng Software* 1998;29(1):1–6.
- [12] Chang JR, Yeih W, Wu YC, Chang JJ. Applications of the complete multiple reciprocity method for solving the 1D Helmholtz equation of a semi-infinite domain. *Adv Eng Software* 2001;32:111–7.
- [13] Yu W, Wang Z, Hong X. Preconditioned multi-zone boundary element analysis for fast 3D electric simulation. *Eng Anal Bound Elem* 2004;28:1035–44.
- [14] Brennan PA, Raver N, Ruehli A. Three dimensional inductance computations with partial element equivalent circuits. *IBM J Res Dev* 1979;23:661–8.
- [15] Wang J, White J. A wide frequency range surface integral formulation for 3-D RLC extraction. Proceedings of the international conference on computer aided-design, 1999. p. 453–7.

- [16] Wang J, A new surface integral formulation of EMQS impedance extraction for 3-D structures. PhD dissertation, Massachusetts Institute of Technology, Cambridge, MA; 1999.
- [17] Zhu Z, Huang J, Song B, White J. Improving the robustness of a surface integral formulation for wide-band impedance extraction of 3-D structures. Proceedings of the international conference on computer aided-design, 2001. p. 592–7.
- [18] Kamiya N, Andoh E. Helmholtz eigenvalue analysis by boundary element method. *J Sound Vib* 1993;160:279–87.
- [19] Dahlquist G, Bjorck A. Numerical methods [Anderson N, Trans.]. Englewood Cliffs, NJ: Prentice-Hall; 1974.
- [20] Forsythe GE, Malcolm MA, Moler CB. Computer methods for mathematical computations. Englewood Cliffs, NJ: Prentice-Hall; 1977.
- [21] Guru BS, Hizioglu HR. Electromagnetic field theory fundamentals. New York: Cambridge University Press; 1998.
- [22] Huang Q, Cruse TA. Some notes on singular integral techniques in boundary element analysis. *Int J Numer Meth Eng* 1993;36: 2643–59.
- [23] Kamon M, Tsuk MJ, White J. Fasthenry: a multipole-accelerated 3-D inductance extraction program. *IEEE Trans Microwave Theory Tech* 1994;42(9):1750–8.